ONLINE SUPPLEMENT

HYPERTENSION-RELATED ALTERATIONS IN WHITE MATTER MICROSTRUCTURE DETECTABLE IN MIDDLE AGE

Linda K. McEvoy, Ph.D[1], Christine Fennema-Notestine, Ph.D[1,2], Lisa T. Eyler Ph.D[3,2], Carol Franz, Ph.D[2], Donald J. Hagler, Jr. Ph.D[1], Michael J. Lyons, Ph.D[4], Matthew S. Panizzon, Ph.D[2], Daniel A Rinker, BA[6], Anders M. Dale, Ph.D[1,5], William S. Kremen, Ph.D[2,7]

1. Department of Radiology, University of California, San Diego (UCSD)
2. Department of Psychiatry, UCSD
3. Mental Illness Research, Education, and Clinical Center, VA San Diego Healthcare System
4. Department of Psychiatry and Brain Sciences, Boston University
5. Department of Neurosciences, UCSD
6. Imaging Genetics Center, Institute for Neuroimaging and Informatics, University of Southern California
7. Center of Excellence for Stress and Mental Health, VA San Diego Healthcare System

Corresponding Author: Linda McEvoy
Department of Radiology,
UCSD,
9500 Gilman Dr, MC 0841
La Jolla, CA, 92093

email: lkmcevoy@ucsd.edu
Ph. (858) 822-6675
Fax: (858) 534-1078

METHODS

Image Acquisition

Images were acquired at two sites, University of California, San Diego (UCSD) and Massachusetts General Hospital (MGH). At UCSD, images were acquired with a GE 3T Discovery 750× scanner (GE Healthcare, Waukesha, WI, USA) with an eight-channel phased array head coil. The imaging protocol included a sagittal 3D fast spoiled gradient echo (FSPGR) T_1-weighted volume optimized for maximum gray/white matter contrast (TE = 3.164 msec, TR = 8.084 msec, TI = 600 msec, flip angle = 8°, pixel bandwidth= 244.141, FOV = 24 cm, frequency = 256, phase = 192, slices = 172, slice thickness = 1.2 mm), and a diffusion-weighted scan with 51 diffusion directions, b value = 1000 s/mm^2, integrated with a pair of b = 0 images with opposite phase-encode polarity, TR = 9700 msec, TE 80-84 msec, pixel bandwidth 3906.25.

At MGH, images were acquired with a Siemens Tim Trio, (Siemens USA, Washington, D.C.) with a 32 channel head coil. The imaging protocol included a 3D magnetization-prepared rapid gradient-echo (MPRAGE) T_1-weighted volume optimized for maximum gray/white matter contrast (TE = 4.33 msec, TR = 2170 msec, TI = 1100 msec, flip angle = 7°, pixel bandwidth= 140, slices = 160, slice thickness = 1.2 mm), and diffusion-weighted scans including two separate b=0 images with opposite phase-encode polarity, followed by two scans with 30 diffusion directions, b value = 1000 s/mm^2 (and one b=0 image), TR = 9500 msec, TE 94 msec, pixel bandwidth 1371.

Image Processing

All imaging processing was performed at UCSD, using procedures that have been previously described in detail[1-3]. Briefly, the T_1-weighted volume was automatically corrected for spatial distortion due to gradient nonlinearity [4] and B_1 field inhomogeneity [5]. Automated volumetric segmentation methods available in the FreeSurfer software suite[6] were used to define grey matter, white matter and cerebral spinal fluid (CSF), and used to constrain fiber tracts as described below.

Diffusion weighted images were corrected for eddy current distortions[7], head motion[8], B_0 distortions (using the reversing gradient method)[9], and gradient nonlinearity distortions[4], and then registered to the T_1-weighted structural image using mutual information[10] after pre-registration using atlas images for each modality. Diffusion images were then rigidly resampled into a standard orientation with 2 mm isotropic resolution. Cubic interpolation was used for all resampling steps. Conventional DTI methods were used to model the diffusion tensor as an ellipsoid where eigenvalues λ_1, λ_2, and λ_3 define the three primary axes[11-14]. Average fractional anisotropy (FA), a scalar value of the degree of anisotropic/directional diffusion within the voxel; mean diffusivity (MD), the average diffusion of all directions; longitudinal diffusivity (LD), the average diffusion along the primary axis and transverse diffusivity (TD), the average diffusion along the two non-primary axes, were calculated. Diffusion metrics for selected fiber tracts were derived using a probabilistic atlas of fiber tract locations and orientations (AtlasTrack [8]). T_1-weighted images were used to nonlinearly register the brain to a common space, and diffusion tensor orientation estimates were compared to the AtlasTrack atlas to obtain a map of the relative probability that a voxel belonged to a particular fiber

given the location and similarity of diffusion orientations. These probability values were used to calculate weighted averages of the diffusion measures for each fiber tract. A fiber probability threshold of 0.08 was used to ensure that voxels with very low probability of belonging to a given fiber did not contribute to average values. This threshold value was previously found to provide optimal correspondence in fiber tract volumes between atlas-derived and manually-selected fiber tract ROIs. Results of FreeSurfer's automated brain segmentation were used to identify and exclude voxels in fiber tract regions of interest that were primarily gray matter or CSF. Left and right hemisphere metrics from homologous tracts were averaged. The nine tracts analyzed here (uncinate fasciculus, UF, inferior frontal occipital fasciculus, IFOF, the inferior and superior lateral fasciculi, ILF and SLF, the cingulum portion of the cingulum bundle, CgC, anterior thalamic radiations, ATR, corticospinal tract, CST, forceps minor and forceps major) were chosen *a priori* based on prior findings of associations with hypertension [15-17]. The anatomical locations of the nine fiber tracks are illustrated in Figure S1.

REFERENCES

1. Fennema-Notestine C, Hagler DJ, Jr., McEvoy LK, Fleisher AS, Wu EH, Karow DS, Dale AM. Structural MRI biomarkers for preclinical and mild alzheimer's disease. *Hum Brain Mapp*. 2009;30:3238-3253.
2. McDonald CR, Leyden KM, Hagler DJ, Kucukboyaci NE, Kemmotsu N, Tecoma ES, Iragui VJ. White matter microstructure complements morphometry for predicting verbal memory in epilepsy. *Cortex*. 2014;58:139-150.
3. Brown TT, Kuperman JM, Chung Y, Erhart M, McCabe C, Hagler DJ, Jr., Venkatraman VK, Akshoomoff N, Amaral DG, Bloss CS, Casey BJ, Chang L, Ernst TM, Frazier JA, Gruen JR, Kaufmann WE, Kenet T, Kennedy DN, Murray SS, Sowell ER, Jernigan TL, Dale AM. Neuroanatomical assessment of biological maturity. *Curr Biol*. 2012;22:1693-1698.
4. Jovicich J, Czanner S, Greve D, Haley E, van der Kouwe A, Gollub R, Kennedy D, Schmitt F, Brown G, Macfall J, Fischl B, Dale A. Reliability in multi-site structural MRI studies: Effects of gradient non-linearity correction on phantom and human data. *Neuroimage*. 2006;30:436-443.
5. Sled JG, Zijdenbos AP, Evans AC. A nonparametric method for automatic correction of intensity nonuniformity in MRI data. *IEEE Trans Med Imaging*. 1998;17:87-97.
6. Fischl B, Salat DH, Busa E, Albert M, Dieterich M, Haselgrove C, van der Kouwe A, Killiany R, Kennedy D, Klaveness S, Montillo A, Makris N, Rosen B, Dale AM. Whole brain segmentation: Automated labeling of neuroanatomical structures in the human brain. *Neuron*. 2002;33:341-355.
7. Zhuang J, Hrabe J, Kangarlu A, Xu D, Bansal R, Branch CA, Peterson BS. Correction of eddy-current distortions in diffusion tensor images using the known directions and strengths of diffusion gradients. *J Magn Reson Imaging*. 2006;24:1188-1193.
8. Hagler DJ, Jr., Ahmadi ME, Kuperman J, Holland D, McDonald CR, Halgren E, Dale AM. Automated white-matter tractography using a probabilistic diffusion tensor atlas: Application to temporal lobe epilepsy. *Hum Brain Mapp*. 2009;30:1535-1547.

9. Holland D, Kuperman JM, Dale AM. Efficient correction of inhomogeneous static magnetic field-induced distortion in echo planar imaging. *Neuroimage*. 2010;50:175-183.
10. Wells WM, 3rd, Viola P, Atsumi H, Nakajima S, Kikinis R. Multi-modal volume registration by maximization of mutual information. *Med Image Anal*. 1996;1:35-51.
11. Basser PJ. Inferring microstructural features and the physiological state of tissues from diffusion-weighted images. *NMR Biomed*. 1995;8:333-344.
12. Basser PJ, Mattiello J, LeBihan D. Estimation of the effective self-diffusion tensor from the NMR spin echo. *J Magn Reson B*. 1994;103:247-254.
13. Le Bihan D, Mangin JF, Poupon C, Clark CA, Pappata S, Molko N, Chabriat H. Diffusion tensor imaging: Concepts and applications. *J Magn Reson Imaging*. 2001;13:534-546
14. Pierpaoli C, Jezzard P, Basser PJ, Barnett A, Di Chiro G. Diffusion tensor MR imaging of the human brain. *Radiology*. 1996;201:637-648.
15. Maillard P, Seshadri S, Beiser A, Himali JJ, Au R, Fletcher E, Carmichael O, Wolf PA, DeCarli C. Effects of systolic blood pressure on white-matter integrity in young adults in the Framingham Heart Study. *Lancet Neurol*. 2012;11:1039-1047.
16. de Groot M, Ikram MA, Akoudad S, Krestin GP, Hofman A, van der Lugt A, Niessen WJ, Vernooij MW. Tract-specific white matter degeneration in aging. The Rotterdam Study. *Alzheimers Dement*. 2015;11:321-330.
17. Gons RA, van Oudheusden LJ, de Laat KF, van Norden AG, van Uden IW, Norris DG, Zwiers MP, van Dijk E, de Leeuw FE. Hypertension is related to the microstructure of the corpus callosum: The RUN DMC Study. *J Alzheimers Dis*. 2012;32:623-631.

Table S1. Demographic and clinical characteristics at Wave 2 of normotensive individuals and individuals with recent-onset or longer duration hypertension. Values are mean (standard deviations) unless otherwise specified.

Characteristic	Normotensive (n=101)	Shorter-Duration Hypertension (n=42)	Longer-Duration Hypertension (n=173)	p-value
Age, yrs	61.8 (2.6)	61.3 (2.7)	61.9 (2.5)	0.12
Education, yrs	14.2 (2.3)	13.7 (2.2)	13.7 (1. 8)	0.11
BMI kg/m^2	27.3 (4.5)	28.5 (4.9)	29.5 (3.9)	<0.001†
Systolic BP, mmHg	119.2 (9.2)	130.8 (15.0)	133.0 (17.7)	<0.001‡
Diastolic BP mmHg	74.4 (6.8)	79.7 (9.7)	80.9 (9.8)	<0.001‡
*log triglycerides, mg/dL	4.65 (0.58)	4.72 (0.58)	4.77 (0.50)	0.239
*log HDL, mg/dL	3.92 (0.26)	3.83 (0.24)	3.86 (0.31)	0.138
*log LDL, mg/dL	4.74 (0.34)	4.57 (0.31)	4.60 (0.32)	0.001‡
*log CRP	0.02 (1.03)	0.62 (1.10)	0.51 (1.01)	<0.001‡
APOE ε4+ (%)	26.7	33.3	22.5	0.327
HTN Meds (%)	0	59.5	72.3	<0.001‡
Statins (%)	23.8	40.5	42.2	0.007‡
Diabetes (%)	5	23.8	16.8	0.003‡
Smoking (% current/former)	21.8 / 33.7	26.2 / 40.5	17.9 / 37.6	0.587
Alcohol (% moderate/ heavy)	53.5 / 6.9	59.5 / 9.5	50.0 / 18.0	0.083

yrs indicates years, BMI body mass index, BP blood pressure, HDL high density lipoprotein; LDL low density lipoprotein; CRP, C-reactive protein; HTN Meds antihypertensive medication.

* Lipid and CRP data were missing for a small number of participants. N's for triglyceride and LDL data for the 3 groups were 94, 40, and 160; N's for HDL were 95, 40, 161; N's for CRP were 97, 42, and 166.

† the longer-duration hypertensive group differed significantly from the normotensive group.

‡ the normotensive group differed from the two hypertensives groups, who did not differ from each other

Table S2. F and p values of the differences in tract-specific diffusion measures between normotensive, and those with shorter or longer duration hypertension, controlling for age, scanner site, and non-independence of twin data.

Fiber Track	FA	MD	TD	LD
UF	**3.72; 0.028**	**8.17; <.001**	**7.13; 0.001**	**4.70; 0.011**
IFOF	2.76; 0.068	2.77; 0.068	3.05; 0.052	1.55; 0.217
ILF	2.53; 0.085	**3.28; 0.042**	**3.71; 0.028**	1.63 0.200
SLF	**5.44; 0.006**	**6.13; 0.003**	**6.83; 0.002**	2.15 0.122
CgC	1.91; 0.154	1.19; 0.310	1.32; 0.271	0.32; 0.726
ATR	**4.65; 0.012**	**4.49; 0.014**	**4.98; 0.009**	2.74; 0.070
FMin	1.85; 0.163	1.54; 0.220	1.57; 0.213	1.39; 0.254
FMaj	1.11; 0.333	0.82; 0.443	0.88; 0.417	0.36; 0.701
CST	0.76; 0.471	0.81; 0.447	0.89; 0.414	1.18; 0.310

Values are from base models which corrected for age, scanner site and non-independence of twin data; p values < .05 are shown in bold; underlined values remained significant after adjustment, in separate models, for education level, alcohol use, BMI, diabetes, CRP levels, LDL levels, and statin use.
FA indicates fractional anisotropy; MD, mean diffusivity; TD, transverse diffusivity; LD, longitudinal diffusivity; htn hypertension; UF, uncinate fasciculi; IFOF, inferior fronto-occipital fasciculi; ILF, the inferior lateral fasciculi; SLF, the superior lateral fasciculi; ATR, anterior thalamic radiations; CgC, cingulum portion of the cingulate bundle; Fmin, forceps minor; Fmaj, forceps major, and CST, corticospinal tract.

Table S3. Demographic and clinical characteristics of normotensive individuals and those with controlled and uncontrolled hypertension. Values shown are mean (standard deviation) unless otherwise specified.

Characteristic	Normotensive (n=101)	Controlled Hypertension (n=142)	Uncontrolled Hypertension (n=73)	p value
Age, yrs	61.8 (2.6)	61.2 (2.5)	61.4 (2.6)	0.254
Education, yrs	14.2 (2.3)	13.6 (1.9)	13.9 (1.9)	0.062
BMI kg/m^2	27.3 (4.5)	28.8 (4.2)	30.4 (3.96)	<0.001†
Systolic BP, mmHg	119.2 (9.2)	123.1 (10.0)	150.9 (12.8)	<0.001†
Diastolic BP mmHg	74.4 (6.8)	76.0 (7.0)	89.8 (8.0)	<0.001‡
*log Triglycerides, mg/dL	4.65 (0.58)	4.73 (0.46)	4.83 (0.62)	0.129
*log HDL, mg/dL	3.9 (0.26)	3.9 (0.3)	3.8 (0.3)	0.147
*log LDL, mg/dL	4.74(0.034)	4.55 (0.028)	4.67 (0.040)	<0.001§
*log CRP	-0.01 (0.98)	0.41 (0.98)	0.55 (0.92)	<0.001‖
APOE e4+ (%)	73.3 / 26.7	73.2 / 26.8	79.5 / 20.5	0.565
HTN Meds (%)	0	81	47.9	<0.001†
Statins (%)	23.8	51.4	23.3	<0.001§
Diabetes (%)	5	22.5	9.6	<0.001§
Smoking (%current/former)	21.8 / 33.7	20.4 / 36.6	17.8 / 41.1	0.896
Alcohol (% moderate/heavy)	53.5 / 6.9	51.8 / 13.5	52.1 / 21.9	0.050‡

For abbreviations, see footnote to Table S2.

* Lipid and CRP data were missing for a small number of participants. The N's for triglycerides for the 3 groups were 94,133,67; N's for LDL were 92, 128, 64; for HDL were 95, 134, and 67; and for CRP were 96, 132, and 69.

† all 3 groups differed significantly from each other

‡ the uncontrolled hypertensive group differed from controlled hypertensive and normotensive groups, who did not differ from each other.

§ the controlled hypertensive group differed from significantly from normotensive and uncontrolled hypertensive groups, who did not differ from each other.

‖ the normotensive group differed from the hypertensive groups, who did not differ from each other.

Table S4. F and p values of the differences in tract-specific diffusion measures between normotensive, controlled and uncontrolled hypertension, controlling for age, scanner site, and non-independence of twin data.

Fiber Track	FA	MD	TD	LD
UF	**3.09; 0.050**	**8.06; <0.001**	**6.65; 0.002**	**4.81; 0.010**
IFOF	2.80; 0.066	2.76; 0.068	3.05; 0.052	1.74; 0.181
ILF	2.04; 0.135	**3.39; 0.038**	**3.53; 0.033**	2.06 0.134
SLF	**5.55; 0.005**	**6.69; 0.002**	**7.32; 0.001**	2.63; 0.077
CgC	1.73; 0.182	1.19; 0.310	1.18; 0.311	0.59; 0.558
ATR	**4.01; 0.021**	**4.55; 0.013**	**4.87; 0.010**	**3.20; 0.045**
Forceps Min	1.75; 0.179	0.72; 0.488	1.14; 0.323	0.09; 0.914
Forceps Maj	1.09; 0.341	0.93; 0.398	0.90; 0.411	0.91; 0.406
CST	1.36; 0.260	0.92; 0.400	1.33; 0.269	0.23; 0.791

Values are from base models which corrected for age, scanner site and non-independence of twin data; p values < .05 are shown in bold; underlined values remained significant with separate adjustment for potentially related variables, including education level, alcohol use, BMI, diabetes, CRP level, LDL level, and use of statins.

For abbreviations, see footnote to Table S2.

SUPPLEMENTAL FIGURES

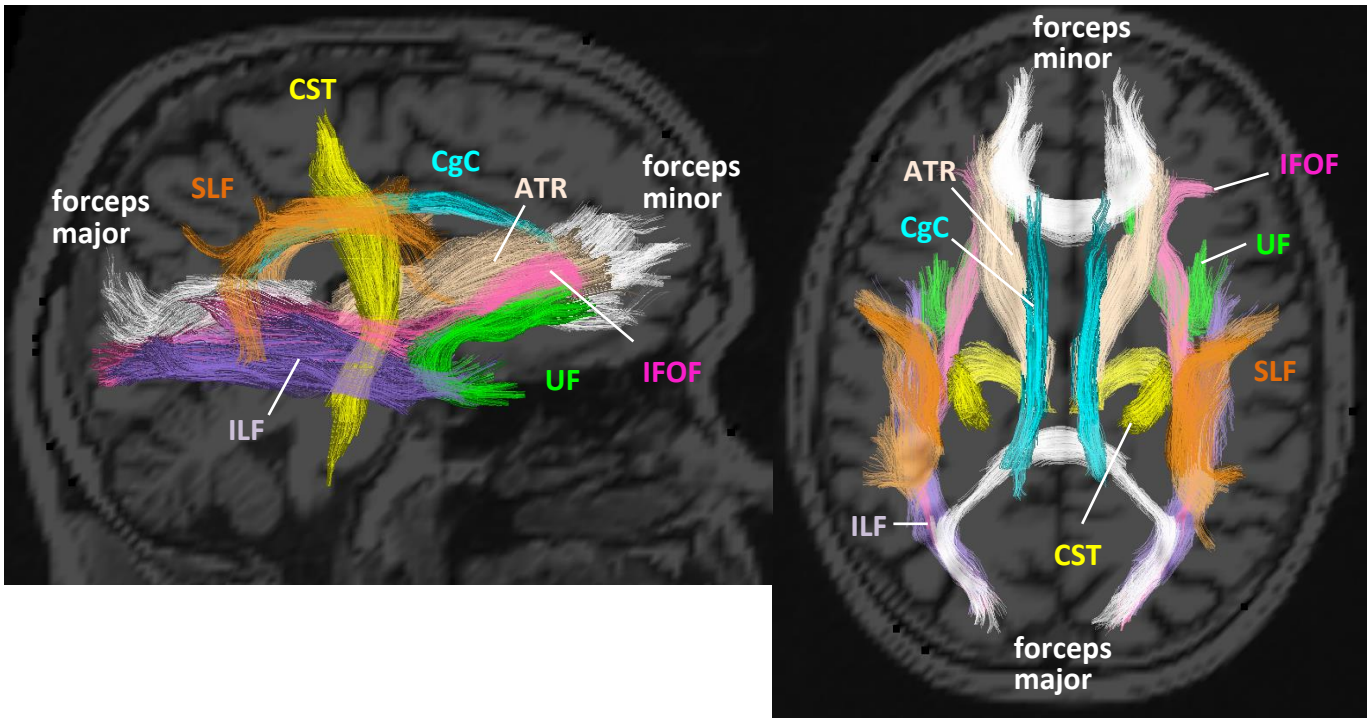

Figure S1. Diagrammatic representation of the anatomical location of the nine fiber tracts examined in this study. View of the tracts from the right side is superimposed on a sagittal brain image (left), view of the tracts from above is superimposed on a horizontal brain image (right). The forceps minor contains commissural fibers connecting homologous regions in left and right frontal lobes; the forceps major contains commissural fibers connecting left and right occipital regions. The corticospinal tract (CST) contains fibers that project from motor cortex to the spinal cord. The anterior thalamic radiations (ATR) connect the thalamus to the frontal lobes. The cingulum portion of the cingulate bundle (CgC) connects anterior and posterior cingulate regions. The superior lateral fasciculus (SLF) connects dorsolateral prefrontal areas to supplementary motor areas, superior temporal areas and occipital cortex. The uncinate fasciculus (UF) connects orbitofrontal cortex to temporopolar and limbic regions. The inferior fronto-occipital fasciculus (IFOF) is a long-range cortical association fiber pathway that connects frontal to occipital cortices. The inferior lateral fasciculus (ILF) connects anterior temporal regions with occipital areas.

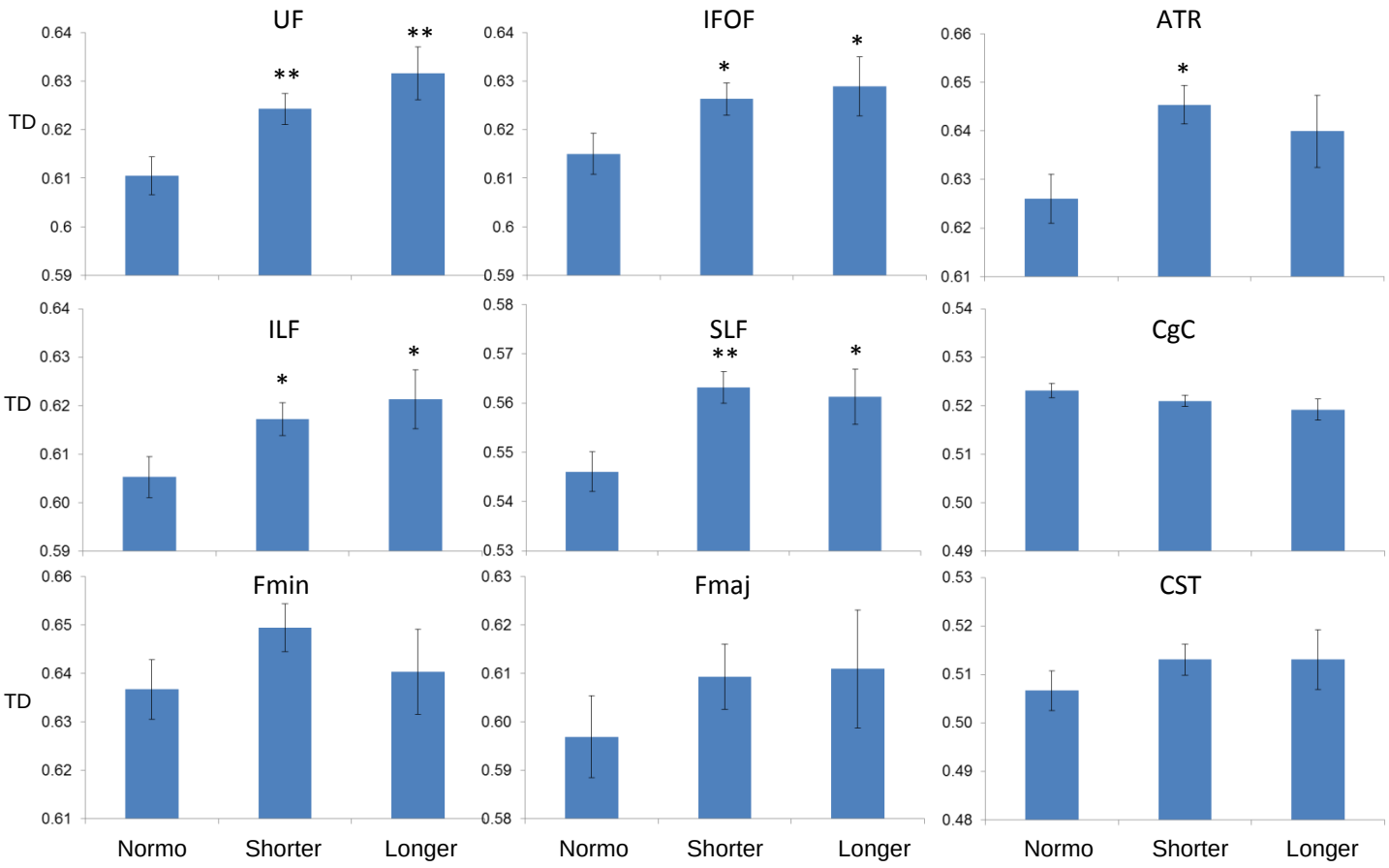

Figure S2. Transverse diffusivity of the nine tracts for normotensive individuals (Normo) and those with longer or shorter duration hypertension. * $p < .05$. ** $p < .01$ for the comparison of the hypertension subgroup with the normotensive group, from the pairwise comparisons within the base model, which controlled for age, scanner site and non-independence of twin data. Longer and shorter duration hypertensive groups did not differ from each other for any measure. For tract abbreviations, see Figure S1.

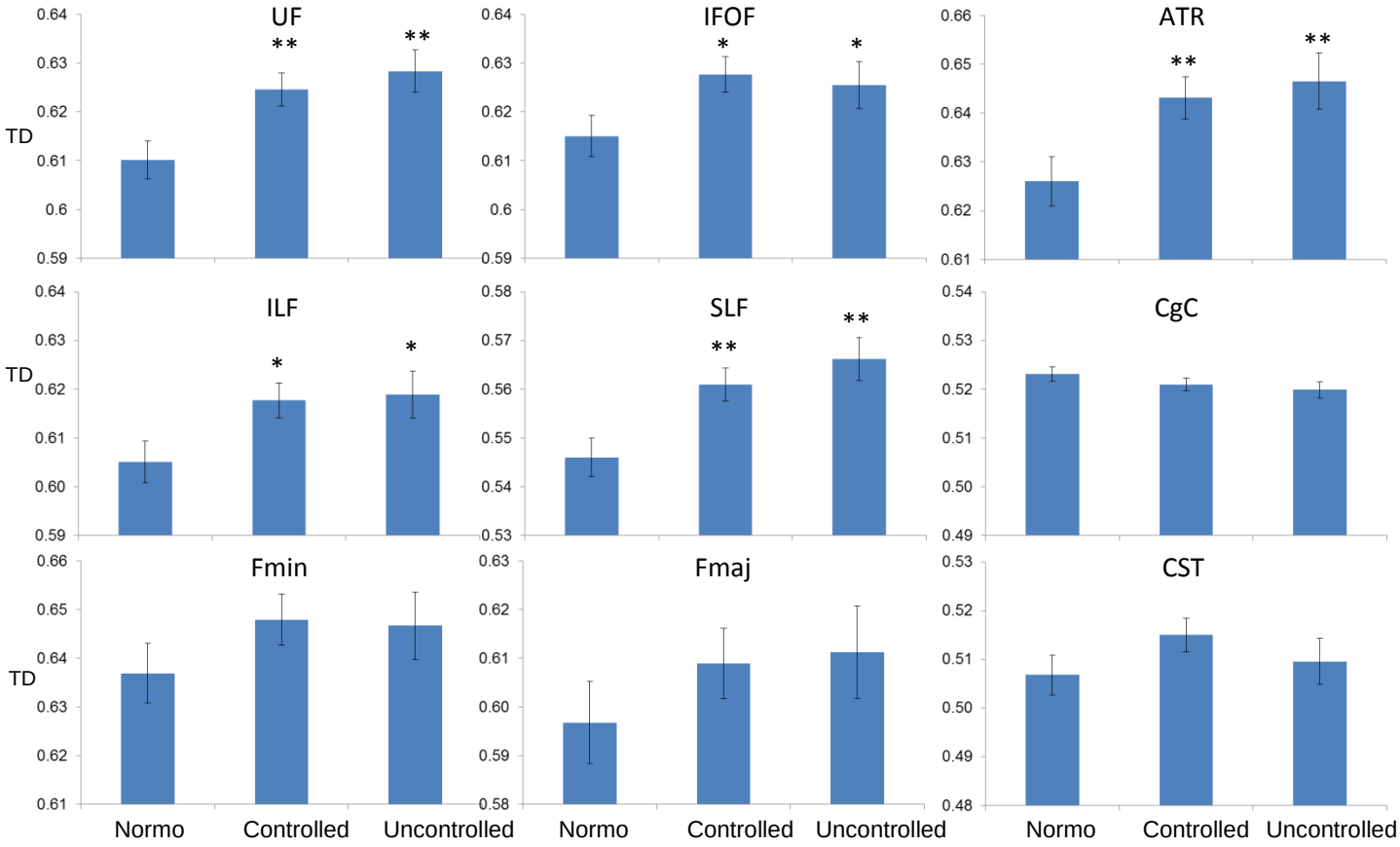

Figure S3. Transverse diffusivity of the nine tracts for normotensive individuals (Normo) and those with controlled or uncontrolled hypertension. * $p < .05$. ** $p < .01$ for the comparison of the hypertensive subgroup with the normotensive group, from the pairwise comparisons within the base model, which controlled for age, scanner site and non-independence of twin data. Controlled and uncontrolled hypertensive groups did not differ from each other for any measure. For tract abbreviations, see Figure S1.